Supporting information for optical forces and torques on eccentric nanoscale core-shell particles

Qiang Sun[1,*], Kishan Dholakia[2,3], and Andrew D Greentree[1]

[1] *Australian Research Council Centre of Excellence for Nanoscale Biophotonics, School of Science, RMIT University, Melbourne, VIC 3001, Australia*

[2] *SUPA, School of Physics and Astronomy, University of St Andrews, North Haugh, Fife KY16 9SS, United Kingdom*

[3] *Department of Physics, College of Science, Yonsei University, Seoul 03722, South Korea*

[*] *Corresponding author: qiang.sun@rmit.edu.au*

Number of pages: 15

Number of figures: 10

Number of tables: 1

SI-1 Optomechanical response of an eccentric spherical core-shell particle under the Gaussian illumination with linear polarisation

Here we provide the detailed optomechanical response of an eccentric spherical core-shell particle under the Gaussian illumination with linear polarisation, as described in Sec. 2 of the main text. The asymmetry of the particle is introduced by the displacement between the core-centre and shell centre. The beam waist radius is set as $w_0 = 1$ μm when the beam propagates along z-axis and polarises along x-axis. The distance between the core-centre and shell-center is h, and the angle from the line connecting core-center and shell-center to the x axis is θ, so that when $\theta = 90^{\text{o}}$ the centre line measured from the shell-centre to the core-centre is along the beam propagation direction.

It is intuitive that the interactions between an eccentric core-shell nanoparticle and external electromagnetic field should be a function of the particle orientation. Take an eccentric Au@SiO_2 particle with the shell radius $a_{\text{shell}} = 90$ nm and core radius $a_{\text{core}} = 60$ nm as an example, when it is under the illumination of a linearly polarised Gaussian beam in air, by using the computational model detailed in Sec. 2 in the main text, Fig. S1 shows the total electric and magnetic fields in the surrounding medium and the transmitted electric and magnetic fields in the particles as the centre of Au core is located at different position relative to the centre of the SiO_2 shell, when the shell centre is fixed at the focus of the beam. The wavelength of the beam is 532 nm, and the displacement between the centre of the Au core and the centre of the SiO_2 shell, $h = 25$ nm. The contour plots of the x component of the electric field in the top row of Fig. S1 indicate that we will expect a force perpendicular to the wave propagation. Also, under a propagating wave, if the particle size is not very small when compared to the light wavelength, the effects of phase across the particle cannot be ignored. Together with the asymmetry given by the eccentric core-shell allocation, a torque acting on this particle will appear as shown by the contour plots of the z component of the electric field and the y component of the magnetic field in the middle and bottom rows of Fig. S1.

The total electric and magnetic fields in the surrounding medium are the superposition of the incident field and the scattered field as $\boldsymbol{E} = \boldsymbol{E}^{\text{inc}} + \boldsymbol{E}^{\text{sca}}$ and $\boldsymbol{H} = \boldsymbol{H}^{\text{inc}} + \boldsymbol{H}^{\text{sca}}$. Introducing the above relationships into Eqs. (4) and (5) in the main text, we notice that the optical force and torque have three parts: one from the indecent field, one from the scattered field and one from the

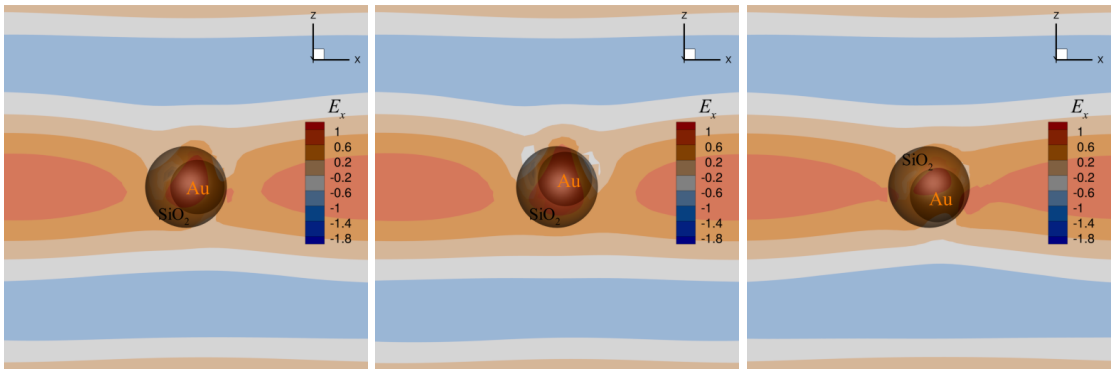

(a) $\theta = 0^o$ (b) $\theta = 45^o$ (c) $\theta = 315^o$

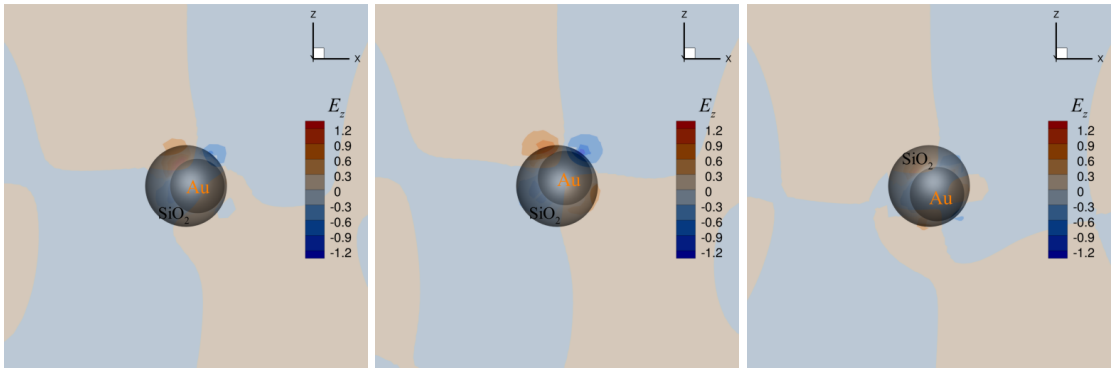

(d) $\theta = 0^o$ (e) $\theta = 45^o$ (f) $\theta = 315^o$

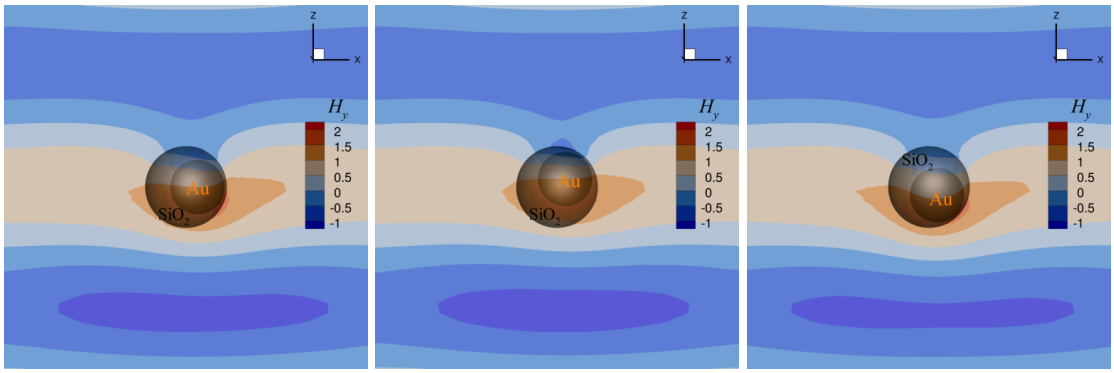

(g) $\theta = 0^o$ (h) $\theta = 45^o$ (i) $\theta = 315^o$

Figure S1: Electric and magnetic fields of when a linearly polarised Gaussian beam is incident on an eccentric Au@SiO_2 core-shell particle in air. The wavelength of the beam is 532 nm and its waist radius is 1 μm. The radius of the Au core is 60 nm, that of the SiO_2 shell is 90 nm, and the displacement between the centre of the Au core and the centre of the SiO_2 shell, $h = 25$ nm. The refractive indices of air, SiO_2 and Au are $n_{\text{air}} = 1.0$, $n_{SiO_2} = 1.46$ and $n_{\text{Au}} = 0.54 + \text{i}2.14$, respectively. (a-c) The x component of the electric field; (d-f) The z component of the electric field; (g-i) The y component of the magnetic field at different orientation of the Au core.

interactions between the scattered and incident fields as

$$F_i^{\mathrm{inc}} = \int_{S_{\mathrm{shell}}} \frac{1}{2}\Big\{\mathrm{Real}\Big[(D_i^{\mathrm{inc}}E_j^{\mathrm{inc},*} + E_i^{\mathrm{inc}}D_j^{\mathrm{inc},*} + B_i^{\mathrm{inc}}H_j^{\mathrm{inc},*} + H_i^{\mathrm{inc}}B_j^{\mathrm{inc},*})n_j - (D_j^{\mathrm{inc}}E_j^{\mathrm{inc},*} + B_j^{\mathrm{inc}}H_j^{\mathrm{inc},*})n_i\Big]\Big\}\mathrm{d}S \tag{S1a}$$

$$F_i^{\mathrm{sca}} = \int_{S_{\mathrm{shell}}} \frac{1}{2}\Big\{\mathrm{Real}\left[(D_i^{\mathrm{sca}}E_j^{\mathrm{sca},*} + E_i^{\mathrm{sca}}D_j^{\mathrm{sca},*} + B_i^{\mathrm{sca}}H_j^{\mathrm{sca},*} + H_i^{\mathrm{sca}}B_j^{\mathrm{sca},*})n_j - (D_j^{\mathrm{sca}}E_j^{\mathrm{sca},*} + B_j^{\mathrm{sca}}H_j^{\mathrm{sca},*})n_i\right]\Big\}\mathrm{d}S \tag{S1b}$$

$$\begin{aligned} F_i^{\mathrm{ext}} = \int_{S_{\mathrm{shell}}} \frac{1}{2}\Big\{\mathrm{Real}\big[&(D_i^{\mathrm{inc}}E_j^{\mathrm{sca},*} + E_i^{\mathrm{inc}}D_j^{\mathrm{sca},*} + B_i^{\mathrm{inc}}H_j^{\mathrm{sca},*} + H_i^{\mathrm{inc}}B_j^{\mathrm{sca},*})n_j \\ &+ (D_i^{\mathrm{sca}}E_j^{\mathrm{inc},*} + E_i^{\mathrm{sca}}D_j^{\mathrm{inc},*} + B_i^{\mathrm{sca}}H_j^{\mathrm{inc},*} + H_i^{\mathrm{sca}}B_j^{\mathrm{inc},*})n_j \\ &- (D_j^{\mathrm{inc}}E_j^{\mathrm{sca},*} + B_j^{\mathrm{inc}}H_j^{\mathrm{sca},*})n_i - (D_j^{\mathrm{sca}}E_j^{\mathrm{inc},*} + B_j^{\mathrm{sca}}H_j^{\mathrm{inc},*})n_i\big]\Big\}\mathrm{d}S \end{aligned} \tag{S1c}$$

$$N_i^{\mathrm{inc}} = \int_{S_{\mathrm{shell}}} \varepsilon_{ijk} r_j^c \frac{1}{2}\Big\{\mathrm{Real}\Big[(D_k^{\mathrm{inc}}E_l^{\mathrm{inc},*} + E_k^{\mathrm{inc}}D_l^{\mathrm{inc},*} + B_k^{\mathrm{inc}}H_l^{\mathrm{inc},*} + H_k^{\mathrm{inc}}B_l^{\mathrm{inc},*})n_l - (D_l^{\mathrm{inc}}E_l^{\mathrm{inc},*} + B_l^{\mathrm{inc}}H_l^{\mathrm{inc},*})n_k\Big]\Big\}\mathrm{d}S \tag{S2a}$$

$$N_i^{\mathrm{sca}} = \int_{S_{\mathrm{shell}}} \varepsilon_{ijk} r_j^c \frac{1}{2}\Big\{\mathrm{Real}\left[(D_k^{\mathrm{sca}}E_l^{\mathrm{sca},*} + E_k^{\mathrm{sca}}D_l^{\mathrm{sca},*} + B_k^{\mathrm{sca}}H_l^{\mathrm{sca},*} + H_k^{\mathrm{sca}}B_l^{\mathrm{sca},*})n_l - (D_l^{\mathrm{sca}}E_l^{\mathrm{sca},*} + B_l^{\mathrm{sca}}H_l^{\mathrm{sca},*})n_k\right]\Big\}\mathrm{d}S \tag{S2b}$$

$$\begin{aligned} N_i^{\mathrm{ext}} = \int_{S_{\mathrm{shell}}} \varepsilon_{ijk} r_j^c \frac{1}{2}\Big\{\mathrm{Real}\big[&(D_k^{\mathrm{inc}}E_l^{\mathrm{sca},*} + E_k^{\mathrm{inc}}D_l^{\mathrm{sca},*} + B_k^{\mathrm{inc}}H_l^{\mathrm{sca},*} + H_k^{\mathrm{inc}}B_l^{\mathrm{sca},*})n_l \\ &+ (D_k^{\mathrm{sca}}E_l^{\mathrm{inc},*} + E_k^{\mathrm{sca}}D_l^{\mathrm{inc},*} + B_k^{\mathrm{sca}}H_l^{\mathrm{inc},*} + H_k^{\mathrm{sca}}B_l^{\mathrm{inc},*})n_l \\ &- (D_l^{\mathrm{inc}}E_l^{\mathrm{sca},*} + B_l^{\mathrm{inc}}H_l^{\mathrm{sca},*})n_k - (D_l^{\mathrm{sca}}E_l^{\mathrm{inc},*} + B_l^{\mathrm{sca}}H_l^{\mathrm{inc},*})n_k\big]\Big\}\mathrm{d}S \end{aligned} \tag{S2c}$$

Based on the numerical experiments set up in our work, since the shell is spherical and its centre is fixed at the focus of the incident Gaussian beam, the force and torque due to the incident fields $\boldsymbol{E}^{\mathrm{inc}}$ and $\boldsymbol{H}^{\mathrm{inc}}$ are zeros: $\boldsymbol{F}^{\mathrm{inc}} = \boldsymbol{0}$ and $\boldsymbol{N}^{\mathrm{inc}} = \boldsymbol{0}$. It is worth mentioning that if the particle is not located at the focus of beam, there will be optical force generated from the incident field (gradient force). As such, in this work, we investigated the total optical force and torque, $\boldsymbol{F}$ and $\boldsymbol{N}$ defined in Eqs. (4) and (5) in the main text, respectively, and those from the scattered field, $\boldsymbol{F}^{\mathrm{sca}}$ and $\boldsymbol{N}^{\mathrm{sca}}$ defined in Eqs. (S1b) and (S2b), respectively, and those from the interaction between the scattered field and the incident field $\boldsymbol{F}^{\mathrm{ext}}$ and $\boldsymbol{N}^{\mathrm{ext}}$ defined in Eqs. (S1c) and (S2c), respectively.

SI-1.1 Optical force along the beam propagation direction

Let us first consider the optical force along the beam propagation or the trapping force. Taking an Au@SiO_2 eccentric core-shell particle with the shell radius $a_{\mathrm{shell}} = 90$ nm and core radius $a_{\mathrm{core}} = 60$ nm which shell centre is at the focal point of the Gaussian beam as an example. Fig. S2 shows how the asymmetry, h, can affect the trapping force F_z and its components F_z^{sca} and F_z^{ext}

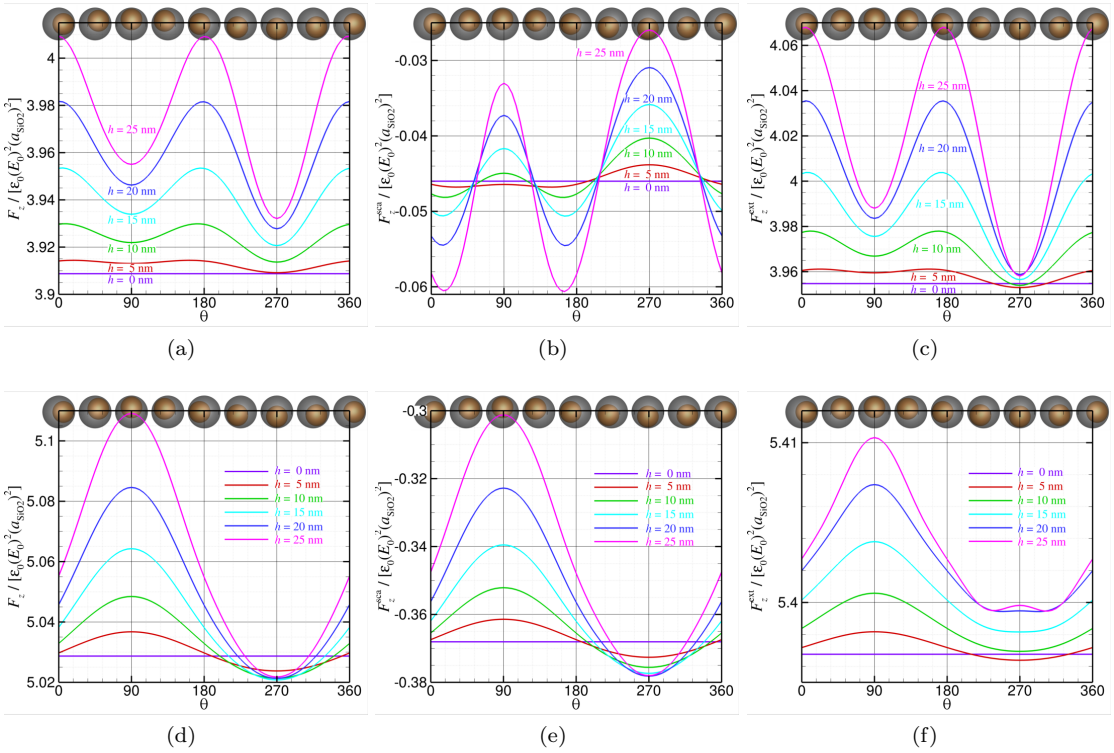

Figure S2: Optical force along the direction of incident beam propagation on the eccentric Au@SiO_2 core-shell particle under the linearly polarised Gaussian beam illumination. (a-c) in air with $n_{\text{air}} = 1$; (d-f) in water with $n_{\text{water}} = 1.33$. The shell radius is $a_{\text{shell}} = 90$ nm, the core radius is $a_{\text{core}} = 60$ nm, the beam wavelength is $\lambda = 532$ nm, and the beam waist radius is $w_0 = 1$ μm.

when an eccentric Au@SiO_2 core-shell particle illuminated by a beam with wavelength $\lambda = 532$ nm. The top row of Fig. S2 shows the variations of F_z , F_z^{sca} and F_z^{ext} along with the Au core orientation, θ when the surrounding medium is air with $n_{\text{air}} = 1$. In Fig. S2(a), we can see that when the distance, h, between the Au core-centre and the SiO_2 shell-centre increases, the total optical force along the wave propagation, F_z becomes larger and larger at all orientation angle θ. It is noticeable that the force curves have two local minima when the orientation angle $\theta = 90^{\text{o}}$ and $\theta = 270^{\text{o}}$, respectively, where F_z is larger at $\theta = 90^{\text{o}}$ compared to that at $\theta = 270^{\text{o}}$. The trends of the optical force along the wave propagation due to the interaction between the scattered field and the incident field, F_z^{ext} behaves the same, as shown in Fig. S2(c). It is noticeable that the magnitude of this part of the optical force, F_z^{ext} is higher than the net optical force, F_z. This is due to the fact that the optical force from the scattered field shows a tractor effect (opposite to the wave propagation direction), as shown in Figs S2(b). Nevertheless, the optical force from the scattered field, F_z^{sca} is much smaller relative to that from the interaction between the incident and the scattered field, F_z^{ext}.

When the surrounding medium is water with $n_{\text{water}} = 1.33$, the variations of the optical forces, F_z due to the asymmetry of the Au core change accordingly because of the difference of the ratio of the relative refractive indices between the SiO_2 shell and the surrounding medium. One obvious difference is that $\theta = 90^{\text{o}}$ becomes the orientation of Au core corresponding to the maximum optical

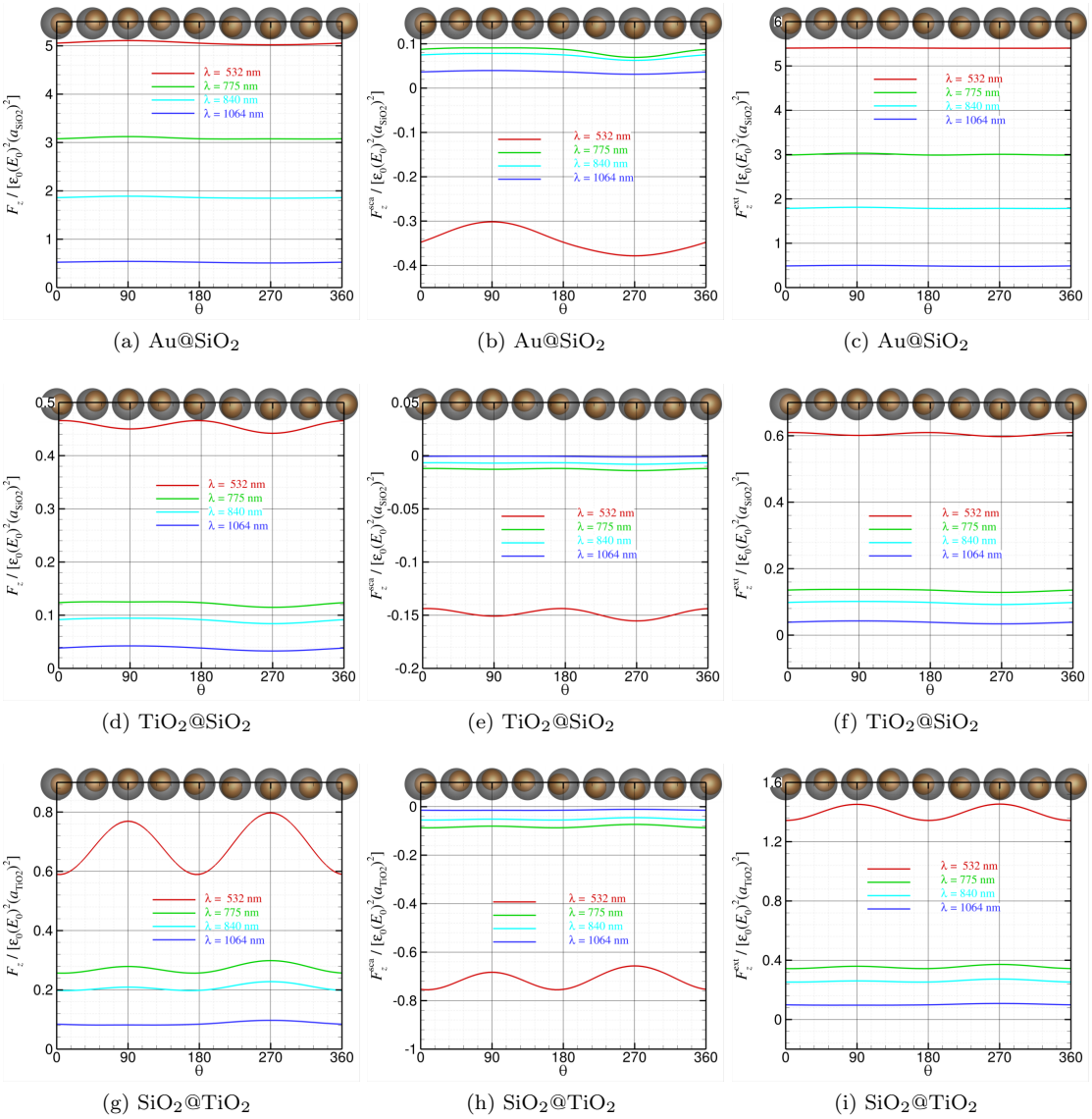

(a) $Au@SiO_2$ (b) $Au@SiO_2$ (c) $Au@SiO_2$

(d) $TiO_2@SiO_2$ (e) $TiO_2@SiO_2$ (f) $TiO_2@SiO_2$

(g) $SiO_2@TiO_2$ (h) $SiO_2@TiO_2$ (i) $SiO_2@TiO_2$

Figure S3: Optical force along the direction of incident beam propagation on three types of eccentric core-shell particles in water under a linearly polarised Gaussian beam illumination with beam waist radius as $w_0 = 1$ μm. The geometrical features of the core-shell particle are $a_{\text{shell}} = 90$ nm, $a_{\text{core}} = 60$ nm and $h = 25$ nm.

force along the wave propagation, as shown in Fig. S2(d). Also, when the asymmetry h of the eccentric particle becomes larger, the net optical force along the beam propagation, F_z increases at most orientations of the Au core except for a small range around $\theta = 270^{\text{o}}$ which is the effect from the force component due to the scattered field, F_z^{sca} as displayed in Fig. S2(e). When comparing Figs. S2(e-f), we can see that the optical force from the interaction between the incident and the scattered field, F_z^{ext} dominates that from the scattered field, F_z^{sca}. Converting the magnitude of the optical trapping force, F_z in Fig. S2(d), we obtain the Q-factor, $Q = F_z\, c/(n_{\text{medium}} P_0)$ with c being the speed of light, larger than 0.029 which is reasonable.

Fig. S3 presents the effect of wavelength on the optical force along the Gaussian beam prop-

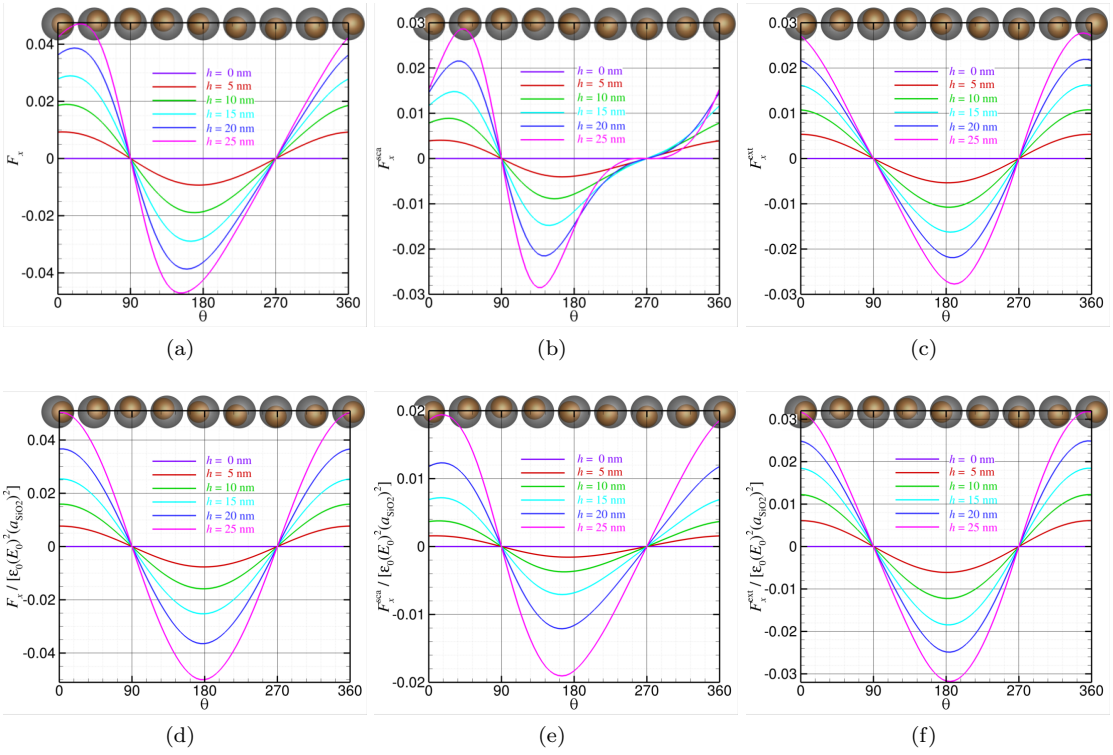

Figure S4: Optical force perpendicular to the direction of incident beam propagation on the eccentric Au@SiO_2 core-shell particle under the linearly polarised Gaussian beam illumination. (a-c) in air with $n_{\text{air}} = 1$; (d-f) in water with $n_{\text{water}} = 1.33$. The shell radius is $a_{\text{shell}} = 90$ nm, the core radius is $a_{\text{core}} = 60$ nm, the beam wavelength is $\lambda = 532$ nm, and the beam waist radius is $w_0 = 1$ μm.

agation for three types of eccentric core-shell particles in water: Au@SiO_2, TiO_2@SiO_2 and SiO_2@TiO_2. Four wavelengths, $\lambda = 532$ nm, $\lambda = 775$ nm, $\lambda = 840$ nm and $\lambda = 1064$ nm are under consideration when the linearly polarised Gaussian beam waist radius is fixed as $w_0 = 1$ μm. As the wavelength becomes larger and larger, the magnitudes of the net optical force, F_z decreases. From the first and second rows of Fig. S3, we can clearly see that the optical force from the interaction between the scattered and incident fields, F_z^{ext} dominates the force from the scattered field, F_z^{sca} for Au@SiO_2 and TiO_2@SiO_2. However, for SiO_2@TiO_2, the magnitude of these two parts are in the same order and they are competing with each other. The net force F_z shown in Fig. S3(g) indicates that the optical force from the interaction between the scattered and incident fields, F_z^{ext} overcomes the force from the scattered field, F_z^{sca}.

SI-1.2 Optical force perpendicular to the beam propagation

As the core particle is not concentric with the centre of the shell, there will be an optical force perpendicular to the beam propagation direction. Fig. S4 displays the optical force perpendicular to a linearly polarised Gaussian beam with its light wavelength as $\lambda = 532$ nm illuminating on an eccentric Au@SiO_2 core-shell particle. We, firstly, would like to point out that compared to the optical force along the beam propagation axis F_z, F_x can be deemed as a secondary effect since

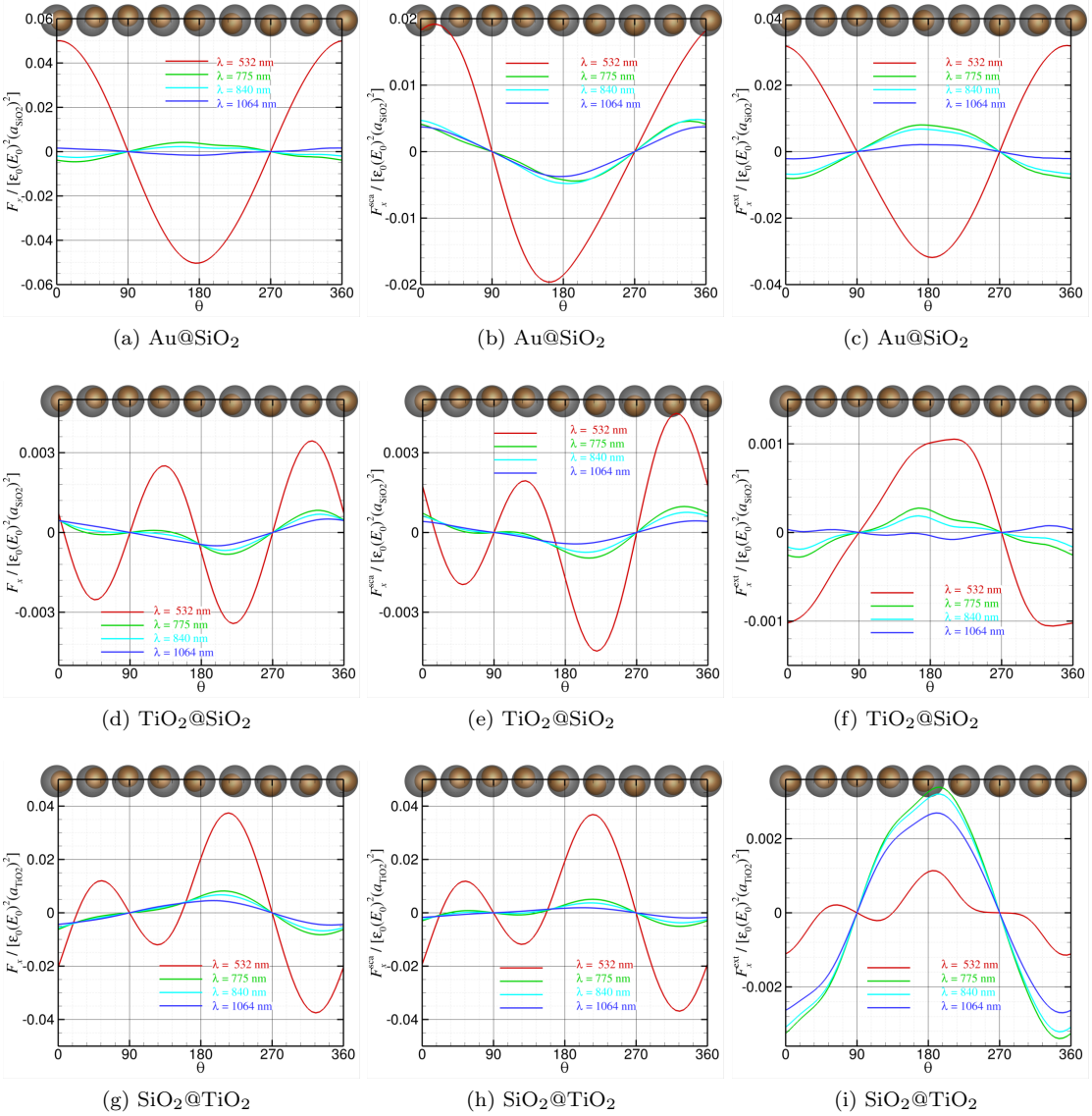

(a) $Au@SiO_2$ (b) $Au@SiO_2$ (c) $Au@SiO_2$

(d) $TiO_2@SiO_2$ (e) $TiO_2@SiO_2$ (f) $TiO_2@SiO_2$

(g) $SiO_2@TiO_2$ (h) $SiO_2@TiO_2$ (i) $SiO_2@TiO_2$

Figure S5: Optical force perpendicular to the direction of incident beam propagation on three types of eccentric core-shell particles in water under a linearly polarised Gaussian beam illumination with beam waist radius as $w_0 = 1$ μm. The geometrical features of the core-shell particle are $a_{\text{shell}} = 90$ nm, $a_{\text{core}} = 60$ nm and $h = 25$ nm.

the magnitude of F_x is 2 orders lower than that of F_z.

The variation trends of such a force, F_x and its components, F_x^{sca} and F_x^{ext} with respect to the orientation of the Au core, θ are quite similar for air or water as the surrounding medium. It is intuitive to consider that the maximum value of this optical force, F_x appears when the core particle is at the maximum displacement from the beam axis at $\theta = 0^{\text{o}}$ and $\theta = 180^{\text{o}}$ which is demonstrated in Fig. S4. If the surrounding medium is air, the orientation of the Au core corresponding to the largest value of F_x is shifted a little away from $\theta = 0^{\text{o}}$ or $\theta = 180^{\text{o}}$ as displayed in S4(a). This is because the change of the refractive index of the surrounding medium tuned the scattered field that consequently affects the optical force, F_x. Unlike the force along the beam propagation, F_z in

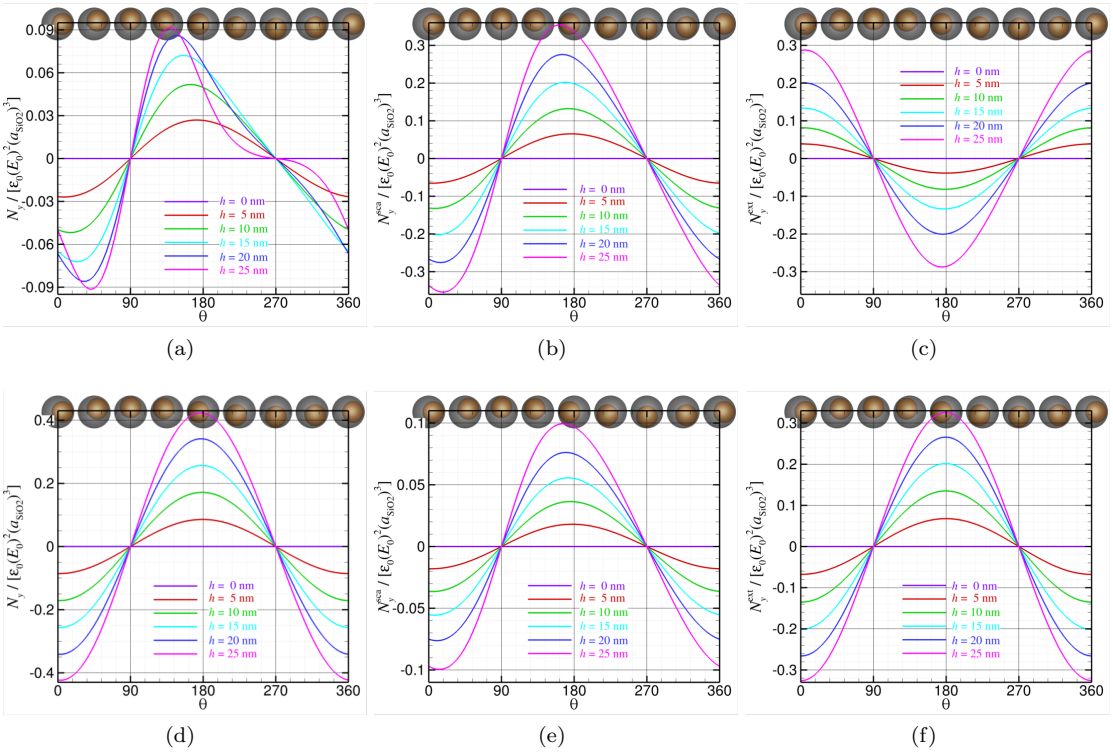

Figure S6: Optical torque perpendicular to the direction of incident beam propagation on the eccentric Au@SiO_2 core-shell particle under the linearly polarised Gaussian beam illumination. (a-c) in air with $n_{\text{air}} = 1$; (d-f) in water with $n_{\text{water}} = 1.33$. The shell radius is $a_{\text{shell}} = 90$ nm, the core radius is $a_{\text{core}} = 60$ nm, the beam wavelength is $\lambda = 532$ nm, and the beam waist radius is $w_0 = 1$ μm.

which the contribution of the interaction between the scattered and incident fields is dominating, for the optical force perpendicular to the beam direction, F_x, both the force from the scattered field, F_x^{sca} and that from the interaction of the scattered and incident fields, F_x^{ext} have similar contributions to the net F_x for the Au@SiO_2 core-shell particle when $\lambda = 532$ nm.

The optical force perpendicular to beam propagation under different wavelengths on three types of eccentric core-shell particles with $h = 25$ nm are shown in Fig. S5. For the Au@SiO_2 core-shell particle at long wavelengths, the force from the scattered field, F_x^{sca} competes with that from the interaction of the scattered and incident fields, F_x^{ext}, as shown in Figs. S5(b-c). As to the TiO_2@SiO_2 and SiO_2@TiO_2 core-shell particles, the net force, F_x is dominated by the contribution from the scattered field, F_x^{sca} for all the wavelengths under consideration, as displayed in the second and third rows of Fig. S5.

SI-1.3 Optical torque

The direction of the optical torque is perpendicular to the plane constructed by the light propagation direction and its electric field polarisation direction. Fig. S6 illustrates how the asymmetry, h and orientation, θ of the Au core affect the optical torque on an eccentric Au@SiO_2 core-shell particle under the illumination of a linearly polarised Gaussian beam with wavelength as $\lambda = 532$ nm.

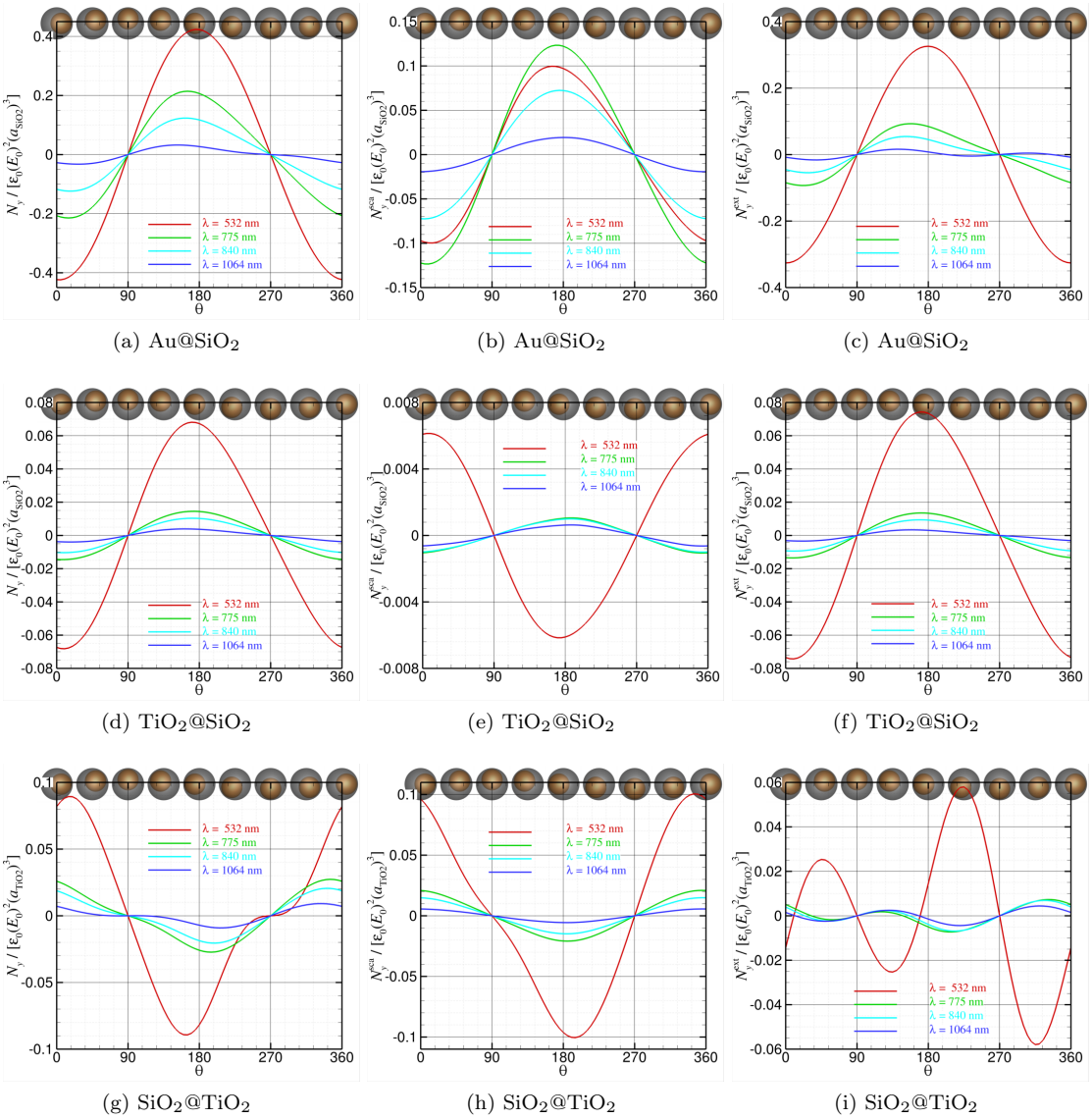

(a) $Au@SiO_2$ (b) $Au@SiO_2$ (c) $Au@SiO_2$

(d) $TiO_2@SiO_2$ (e) $TiO_2@SiO_2$ (f) $TiO_2@SiO_2$

(g) $SiO_2@TiO_2$ (h) $SiO_2@TiO_2$ (i) $SiO_2@TiO_2$

Figure S7: Optical torque perpendicular to the direction of incident beam propagation on three types of eccentric core-shell particles in water under a linearly polarised Gaussian beam illumination with beam waist radius as $w_0 = 1$ μm. The geometrical features of the core-shell particle are $a_{\text{shell}} = 90$ nm, $a_{\text{core}} = 60$ nm and $h = 25$ nm.

As shown in Figs. S6(b-c) and (e-f), when the displacement h between the centre of the Au core and that of the SiO_2 shell increases, the optical torques due to the scattered field and the interaction between the incident and scattered fields become more and more significant. However, these two effects are out of phase (180 degree difference) along the orientation angle of the Au core, θ, when the surrounding medium is air, as shown in Figs. S6(b) and (c). This leads to a small net optical torque as presented in Fig. S6(a). When the surrounding medium is water, the optical torques due to the scattered field and the interaction between the incident and scattered fields are in phase along with the orientation angle of the Au core, θ. As such, the total optical torque on the eccentric $Au@SiO_2$ core-shell particle in water is more significant relative to that in air.

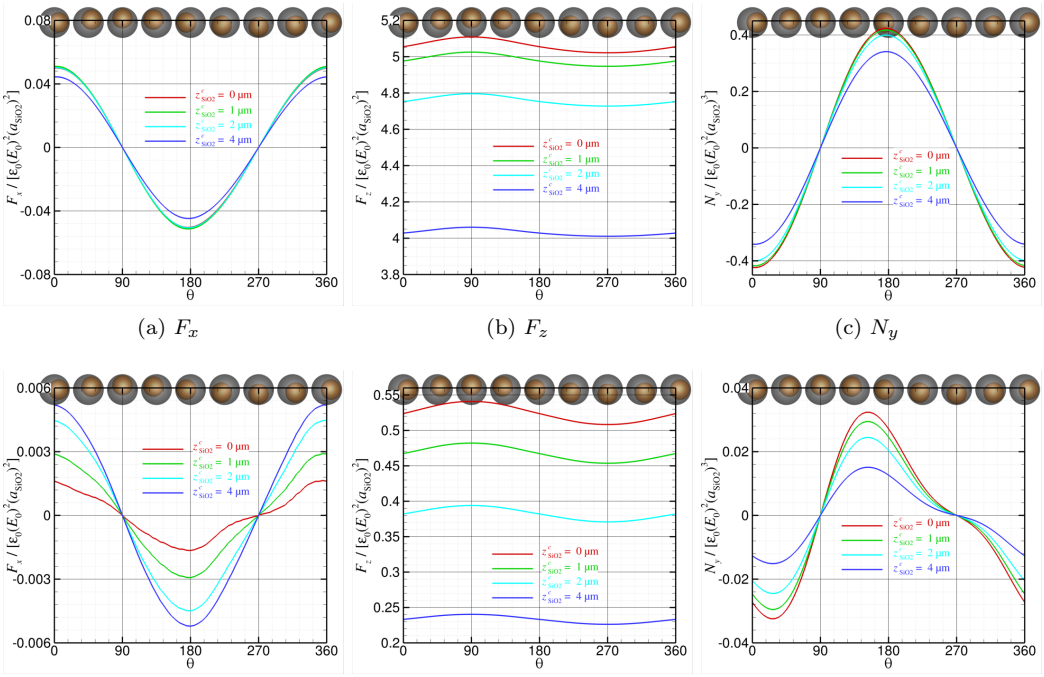

(a) F_x (b) F_z (c) N_y

(d) F_x (e) F_z (f) N_y

Figure S8: Optical force and torque an eccentric Au@SiO_2 core-shell particle in water ($n_{\text{medium}} = 1.33$) under a circular polarised Gaussian beam illumination with beam waist radius as $w_0 = 1$ μm when the geometric centre of the shell locates at different positions along the beam propagation direction: (a-c) λ=532 nm and (d-f) λ=1064 nm. The geometric features of the eccentric core-shell particle are $a_{\text{shell}} = 90$ nm, $a_{\text{core}} = 60$ nm and $h = 25$ nm.

Fig. S7 shows the effect of wavelength on the optical torque acting on three types of eccentric core-shell particles with $h = 25$ nm under the illumination of a linearly polarised Gaussian beam in water. As displayed in the first row of Fig. S7, for the Au@SiO_2 eccentric core-shell particle, the optical torque from the scattered field, N_y^{sca} and that from the interaction between the scattered and incident fields, N_y^{ext} are in phase with respect to the orientation of the Au core, θ, which leads to a significant net optical torque, N_y. As to the TiO_2@SiO_2 eccentric core-shell particle, net optical torque, N_y is dominated by the interaction between the scattered and incident fields, N_y^{ext}; while for the SiO_2@TiO_2 eccentric core-shell particle, the contribution from the scattered field dominates.

SI-1.4 When the eccentric core-shell particle is away from the focal point of the beam

In the previous sections, we demonstrate the optomechanical response of an eccentric spherical core-shell particle under the linearly polarised Gaussian illumination when the centre of the shell is trapped at the focus of the beam. Nevertheless, in practice, the optical trapping location of the particle is not at the focal point of beam in most cases due to the field gradient. We then consider a few cases when the geometrical centre of the eccentric core-shell particle is at different

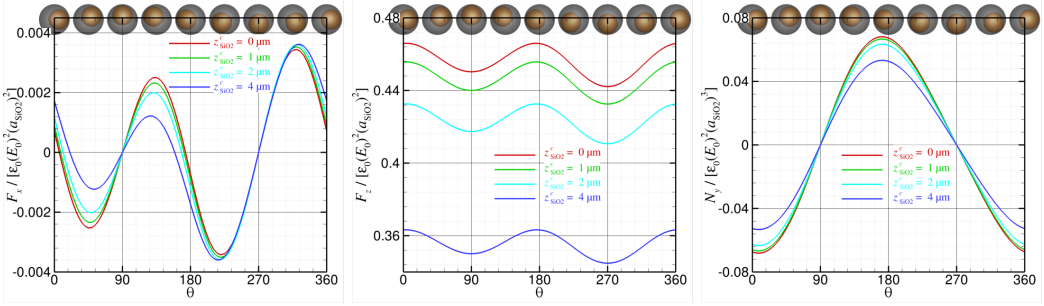

(a) F_x (b) F_z (c) N_y

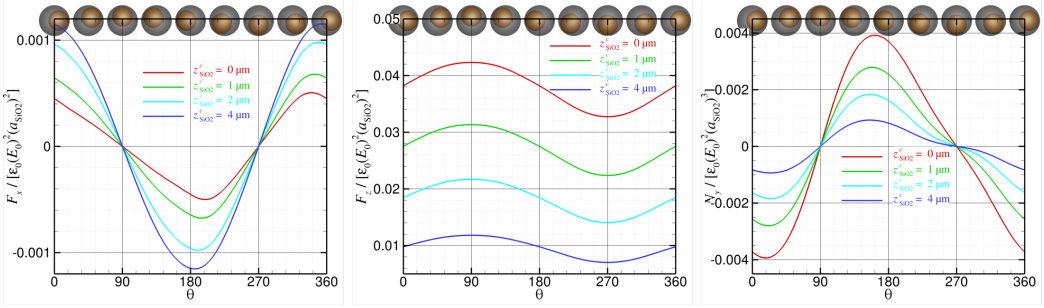

(d) F_x (e) F_z (f) N_y

Figure S9: Optical force and torque an eccentric TiO_2@SiO_2 core-shell particle in water ($n_{\text{medium}} = 1.33$) under a circular polarised Gaussian beam illumination with beam waist radius as $w_0 = 1$ μm when the geometric centre of the shell locates at different positions along the beam propagation direction: (a-c) λ=532 nm and (d-f) λ=1064 nm. The geometric features of the eccentric core-shell particle are $a_{\text{shell}} = 90$ nm, $a_{\text{core}} = 60$ nm and $h = 25$ nm.

positions relative to the beam focus along the beam propagation direction, denoted as $(0, 0, z^c_{\text{shell}})$. From Figs. S8 and S9, we can see that the magnitude of the trapping force F_z changes significantly when z^c_{shell} varies from $z^c_{\text{shell}} = 0$ μm to $z^c_{\text{shell}} = 1$ μm, $z^c_{\text{shell}} = 2$ μm and $z^c_{\text{shell}} = 4$ μm, while the magnitude of the optical torque N_y does not show an obvious variation. This indicates that the optical rotation of nanoscale eccentric core-shall particles should be observable in realistic experiments using current technology.

SI-2 Optical torques on an eccentric spherical core-shell particle under a Gaussian beam with circular polarisation

Circularly polarised Gaussian beams have commonly been used to optically rotate microscale birefringent particles. In this section, we explore the optical torques acting on an eccentric core-shell particle under the Gaussian illumination with circular polarisation. Suppose a circularly polarised beam with Gaussian profile propagates along z direction, such a beam can be described

as:

$$E_x^{\mathrm{inc}} = \frac{\sqrt{2}}{2}E_0\Big\{1+s^2(-\varrho^2\vartheta^2-\mathrm{i}\varrho^4\vartheta^3-2\vartheta^2\xi^2) + s^4\left[2\varrho^4\vartheta^4+3\mathrm{i}\varrho^6\vartheta^5-0.5\varrho^8\vartheta^6+(8\varrho^2\vartheta^4+2\mathrm{i}\varrho^4\vartheta^5)\xi^2\right]\Big\}\psi_0 e^{\mathrm{i}kz} + \frac{\mathrm{i}\sqrt{2}}{2}E_0\left\{s^2(-2\vartheta^2\xi\eta)+s^4\left[8\varrho^2\vartheta^4+2\mathrm{i}\varrho^4\vartheta^5)\xi\eta\right]\right\}\psi_0 e^{\mathrm{i}kz}, \tag{S3a}$$

$$E_y^{\mathrm{inc}} = \frac{\sqrt{2}}{2}E_0\left\{s^2(-2\vartheta^2\xi\eta)+s^4\left[8\varrho^2\vartheta^4+2\mathrm{i}\varrho^4\vartheta^5)\xi\eta\right]\right\}\psi_0 e^{\mathrm{i}kz} + \frac{\mathrm{i}\sqrt{2}}{2}E_0\Big\{1+s^2(-\varrho^2\vartheta^2-\mathrm{i}\varrho^4\vartheta^3-2\vartheta^2\eta^2) + s^4\left[2\varrho^4\vartheta^4+3\mathrm{i}\varrho^6\vartheta^5-0.5\varrho^8\vartheta^6+(8\varrho^2\vartheta^4+2\mathrm{i}\varrho^4\vartheta^5)\eta^2\right]\Big\}\psi_0 e^{\mathrm{i}kz}, \tag{S3b}$$

$$E_z^{\mathrm{inc}} = \frac{\sqrt{2}}{2}E_0\left\{s(-2\vartheta\xi)+s^3\left[(6\varrho^2\vartheta^3+2\mathrm{i}\varrho^4\vartheta^4)\xi\right] + s^5\left[-20\varrho^4\vartheta^5-10\mathrm{i}\varrho^6\vartheta^6+\varrho^8\vartheta^7\right]\xi\right\}\psi_0 e^{\mathrm{i}kz} + \frac{\mathrm{i}\sqrt{2}}{2}E_0\left\{s(-2\vartheta\eta)+s^3\left[(6\varrho^2\vartheta^3+2\mathrm{i}\varrho^4\vartheta^4)\eta\right] + s^5\left[-20\varrho^4\vartheta^5-10\mathrm{i}\varrho^6\vartheta^6+\varrho^8\vartheta^7\right]\eta\right\}\psi_0 e^{\mathrm{i}kz}, \tag{S3c}$$

$$H_x^{\mathrm{inc}} = \frac{\sqrt{2}}{2}\frac{k}{\mu_0\mu\omega}E_0\left\{s^2(-2\vartheta^2\xi\eta)+s^4\left[8\varrho^2\vartheta^4+2\mathrm{i}\varrho^4\vartheta^5)\xi\eta\right]\right\}\psi_0 e^{\mathrm{i}kz} - \frac{\mathrm{i}\sqrt{2}}{2}\frac{k}{\mu_0\mu\omega}E_0\Big\{1+s^2(-\varrho^2\vartheta^2-\mathrm{i}\varrho^4\vartheta^3-2\vartheta^2\xi^2) + s^4\left[2\varrho^4\vartheta^4+3\mathrm{i}\varrho^6\vartheta^5-0.5\varrho^8\vartheta^6+(8\varrho^2\vartheta^4+2\mathrm{i}\varrho^4\vartheta^5)\xi^2\right]\Big\}\psi_0 e^{\mathrm{i}kz}, \tag{S3d}$$

$$H_y^{\mathrm{inc}} = \frac{\sqrt{2}}{2}\frac{k}{\mu_0\mu\omega}E_0\Big\{1+s^2(-\varrho^2\vartheta^2-\mathrm{i}\varrho^4\vartheta^3-2\vartheta^2\eta^2) + s^4\left[2\varrho^4\vartheta^4+3\mathrm{i}\varrho^6\vartheta^5-0.5\varrho^8\vartheta^6+(8\varrho^2\vartheta^4+2\mathrm{i}\varrho^4\vartheta^5)\eta^2\right]\Big\}\psi_0 e^{\mathrm{i}kz} - \frac{\mathrm{i}\sqrt{2}}{2}\frac{k}{\mu_0\mu\omega}E_0\left\{s^2(-2\vartheta^2\xi\eta)+s^4\left[8\varrho^2\vartheta^4+2\mathrm{i}\varrho^4\vartheta^5)\xi\eta\right]\right\}\psi_0 e^{\mathrm{i}kz}, \tag{S3e}$$

$$
\begin{aligned}
H_z^{\mathrm{inc}} = \; & \frac{\sqrt{2}}{2}\frac{k}{\mu_0\mu\omega}E_0\left\{s(-2\vartheta\eta)+s^3\left[(6\varrho^2\vartheta^3+2\mathrm{i}\varrho^4\vartheta^4)\eta\right]\right. \\
& \left.+\, s^5\left[-20\varrho^4\vartheta^5-10\mathrm{i}\varrho^6\vartheta^6+\varrho^8\vartheta^7\right]\eta\right\}\psi_0 e^{\mathrm{i}kz} \\
& -\frac{\mathrm{i}\sqrt{2}}{2}\frac{k}{\mu_0\mu\omega}E_0\left\{s(-2\vartheta\xi)+s^3\left[(6\varrho^2\vartheta^3+2\mathrm{i}\varrho^4\vartheta^4)\xi\right]\right. \\
& \left.+\, s^5\left[-20\varrho^4\vartheta^5-10\mathrm{i}\varrho^6\vartheta^6+\varrho^8\vartheta^7\right]\xi\right\}\psi_0 e^{\mathrm{i}kz}, \qquad \text{(S3f)}
\end{aligned}
$$

Using Eq. (S3) as the incident field and following the simulation demonstrated in Sec. 2 of the main text, we can get the optomechanical response of an eccentric core-shell particle under the illumination of a Gaussian beam with circular polarisation.

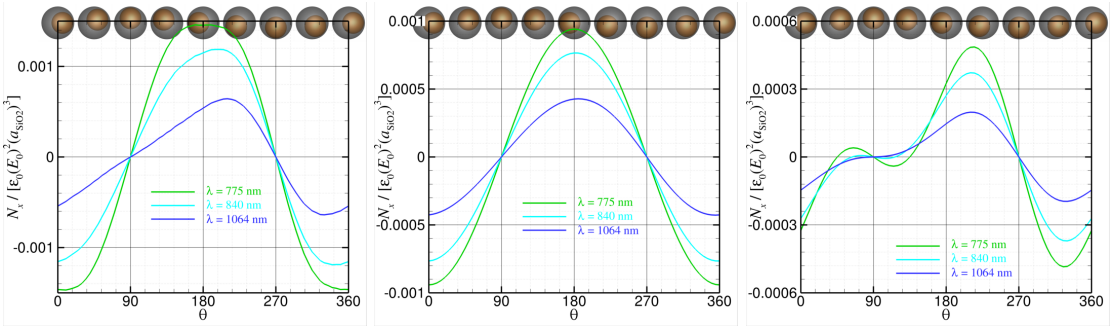

(a) $a_{\mathrm{shell}} = 90$ nm, $a_{\mathrm{core}} = 60$ nm, $h = 25$ nm (b) $a_{\mathrm{shell}} = 90$ nm, $a_{\mathrm{core}} = 60$ nm, $h = 10$ nm (c) $a_{\mathrm{shell}} = 45$ nm, $a_{\mathrm{core}} = 30$ nm, $h = 10$ nm

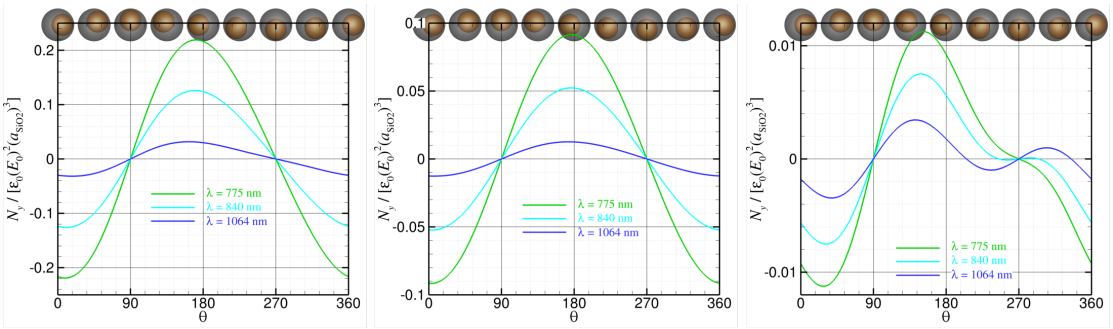

(d) $a_{\mathrm{shell}} = 90$ nm, $a_{\mathrm{core}} = 60$ nm, $h = 25$ nm (e) $a_{\mathrm{shell}} = 90$ nm, $a_{\mathrm{core}} = 60$ nm, $h = 10$ nm (f) $a_{\mathrm{shell}} = 45$ nm, $a_{\mathrm{core}} = 30$ nm, $h = 10$ nm

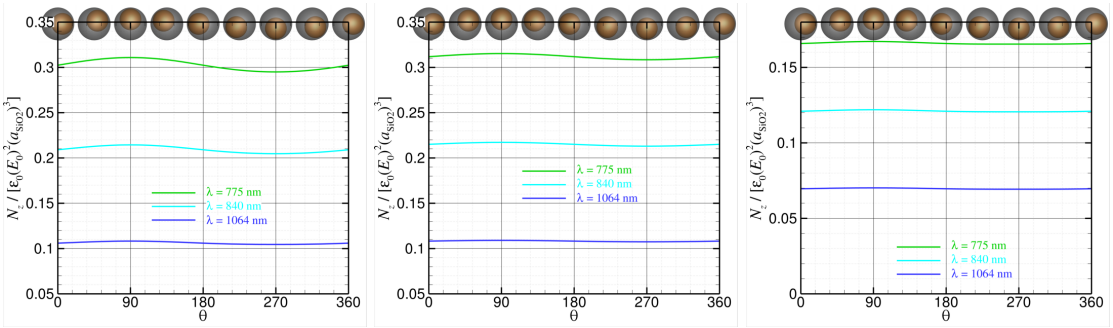

(g) $a_{\mathrm{shell}} = 90$ nm, $a_{\mathrm{core}} = 60$ nm, $h = 25$ nm (h) $a_{\mathrm{shell}} = 90$ nm, $a_{\mathrm{core}} = 60$ nm, $h = 10$ nm (i) $a_{\mathrm{shell}} = 45$ nm, $a_{\mathrm{core}} = 30$ nm, $h = 10$ nm

Figure S10: Optical torques on an eccentric Au@SiO_2 core-shell particle in water with $n_{\mathrm{medium}} = 1.33$ under a circular polarised Gaussian beam illumination with beam waist radius as $w_0 = 1$ μm.

Table S1: **Non-dimensional optical torque $\hat{N}_z \equiv N_z/[\epsilon_0 E_0^2 (a_{\mathbf{SiO_2}})^3]$ on concentric Au@SiO_2 core-shell particle ($h = 0$) under the illumination of Gaussian beam with circular polarisation and waist radius as 1μm in water at different wavelengths, λ, and the corresponding rotation frequency Ω (in Hz) when the beam power is $P_0 = 20$ mW.**

	a_{shell}=90 nm, a_{shell}=45 nm								a_{shell}=60 nm, a_{shell}=30 nm							
	z^c=0 μm		z^c=1 μm		z^c=2 μm		z^c=4 μm		z^c=0 μm		z^c=1 μm		z^c=2 μm		z^c=4 μm	
	$\hat{N}_z$	Ω	$\hat{N}_z$	Ω	$\hat{N}_z$	Ω	$\hat{N}_z$	Ω	$\hat{N}_z$	Ω	$\hat{N}_z$	Ω	$\hat{N}_z$	Ω	$\hat{N}_z$	Ω
λ=775 nm	0.313	594	0.303	575	0.276	523	0.202	383	0.169	314	0.163	303	0.148	275	0.109	202
λ=840 nm	0.216	407	0.208	392	0.186	350	0.131	247	0.123	227	0.118	218	0.106	195	0.075	138
λ=1064 nm	0.109	205	0.102	192	0.086	162	0.053	99	0.070	125	0.066	118	0.056	100	0.035	62

As discussed in the main text, to compare with the case of birefringent particles, we calculated the optical torque on a nanoscale eccentric spherical core-shell particle which is composed by a dielectric core and a dielectric shell, such as TiO_2@SiO_2 and SiO_2@TiO_2. Our results show that the optical torque that is perpendicular the beam direction due to the asymmetry of the eccentric spherical core-shell particle is much higher than the optical torque along the wave propagation direction due to the circular polarisation of the beam.

We also consider another type of eccentric spherical core-shell particle that has a metallic core in a dielectric shell, for example Au@SiO_2. Fig. S10 demonstrates how the optical torques acting on an eccentric spherical Au@SiO_2 core-shell particle in water ($n_{\text{medium}} = 1.33$) change with respect to the orientation of the Au core, θ, when the geometrical centre of the SiO_2 shell is trapped at the beam focus. Due to the eccentricity and refractive index profile, torques N_x and N_y appear and vary with respect to θ. In our simulations, as the eccentric feature (asymmetry), θ, varies in the xz plane, N_y is the dominating torque relative to N_x, as shown in the first and second rows of Fig. S10. Comparing Fig. S10 (d) and Fig. S7 (a), we can see that the amplitude of N_y under the circularly polarised Gaussian illumination is in the same order as that under the linearly polarised Gaussian beam. Due to the circular polarisation, the torque along the wave propagation, N_z, also appears. As shown in the third row of Fig. S10, the magnitude of N_z is in the same order as N_y. Such an enhanced torque N_z acting on the Au@SiO_2 eccentric spherical core-shell particle relative to that on the TiO_2@SiO_2 eccentric spherical core-shell particle is mainly due to the strong absorption of the Au core at the wavelengths under consideration. We would like also to mention that the noticeable optical torque N_z acting on such a Au@SiO_2 particle by using the circular polarisation beam can be achievable when using the concentric core-shell particle, as listed in Table S1. Nevertheless, the rotation of a fully symmetric particle is hard to observe from its steady scattered pattern at the far field, which makes it not an ideal probe for the local measurement of nanoscale environments.